Earth Planet. Sci. Lett. 671 (2025) 119625

Contents lists available at ScienceDirect

Earth and Planetary Science Letters

journal homepage: www.elsevier.com/locate/epsl

A massive primordial atmosphere on early Mars

Sarah Joiret [a,*], Alessandro Morbidelli [a,b], Rafael de Sousa Ribeiro [c], Guillaume Avice [d], Paolo Sossi [e]

[a] Collège de France, Université PSL, 75005 Paris, France
[b] Laboratoire Lagrange, Université Cote d'Azur, CNRS, Observatoire de la Côte d'Azur, Boulevard de l'Observatoire, 06304 Nice Cedex 4, France
[c] Sao Paulo State University, UNESP, Campus of Guaratingueta, Av. Dr. Ariberto Pereira da Cunha, 333 - 6 Pedregulho, Guaratingueta - SP, 12516-410, Brazil
[d] Université Paris Cité, Institut de physique du globe de Paris, CNRS, 75005 Paris, France
[e] Institute of Geochemistry and Petrology, ETH Zürich, Sonneggstrasse 5, CH-8092 Zürich, Switzerland

ARTICLE INFO

Editor: O. Mousis

Keywords:
Mars
Comets
Atmosphere
Noble gases

ABSTRACT

Mars finished forming while the solar nebula was still present, and acquired its primordial atmosphere from this reservoir. The absence of a detectable cometary xenon signature in the present-day Martian atmosphere suggests that the capture of solar nebular gas was significant enough to dilute later cometary contributions. By quantifying the mass of cometary material efficiently retained on Mars, we place a lower bound on the mass of the primordial Martian atmosphere. To test the robustness of our conclusions, we use cometary bombardment data from two independent studies conducted within a solar system evolutionary model consistent with its current structure. Our calculations show that, even under the most conservative scenario, the minimal mass of the primordial martian atmospheres would yield a surface pressure of no less than 2.9 bar. Such a massive nebular envelope is consistent with recent models in which atmospheric capture is strongly enhanced by the presence of heavier species on Mars - due to outgassing or redox buffering with a magma ocean.

1. Introduction

Mars formed rapidly within the first 4 million years of the solar system (Dauphas and Pourmand, 2011), while the solar nebula was still present (Haisch et al., 2001; Wang et al., 2017; Weiss et al., 2021). Heavy noble gas isotopes, which are key tracers of planetary volatile evolution (Pepin, 1992), indicate that Mars acquired its atmosphere from this nebular reservoir. Both in situ measurements (Conrad et al., 2016) and mass spectrometry analyses of Martian meteorites (Ott, 1988; Mathew et al., 1998; Avice et al., 2018) confirm that atmospheric krypton (Kr) and xenon (Xe) have a solar origin. In contrast, the Kr isotopic composition of the Martian mantle is chondritic (Péron and Mukhopadhyay, 2022), ruling out magma ocean outgassing or interior fractionation as main sources of the solar-like noble gas signature in the atmosphere. Instead, these gases were directly accreted from the solar nebula after Mars' mantle rapidly formed from chondritic material.

Sometime after the dispersal of the nebula, a dynamical instability among the giant planets scattered comets into the inner solar system (Tsiganis et al., 2005; Gomes et al., 2005; Nesvorný, 2018). This cometary bombardment reshaped the volatile inventories of the terrestrial planets (Joiret et al., 2023). On Earth, cometary Xe appears in the primordial Xe signature of the atmosphere (Marty et al., 2017). Mars, however, shows no evidence of such cometary Xe signature (Conrad et al., 2016; Péron and Mukhopadhyay, 2022). This difference likely stems from Earth's last giant impacts occurring *after* solar nebula dispersal - erasing most of the solar signatures in Earth's atmosphere - whereas Mars finished forming *before* nebula dispersal (Avice et al., 2018). Mars must have accreted solar nebular gas with high efficiency, as its atmospheric Xe retained a predominantly solar signature despite later cometary bombardment. Efficient capture of solar nebular gas could also account for the elevated neon (Ne) abundance inferred in the Martian mantle (Kurokawa et al., 2021). In this study, we quantify the mass of the cometary bombardment on Mars from dynamical constraints, providing a lower bound on the mass of the solar nebula that early Mars must have accreted to overwhelm any cometary Xe signature.

2. Minimal mass of the primordial atmosphere on Mars

We set the lower bound on the mass of the primordial Martian atmosphere, starting from a robust estimate of the cometary mate-

* Corresponding author.
E-mail address: sarah.joiret@college-de-france.fr (S. Joiret).

https://doi.org/10.1016/j.epsl.2025.119625
Received 25 April 2025; Received in revised form 1 September 2025; Accepted 4 September 2025

Available online 17 September 2025

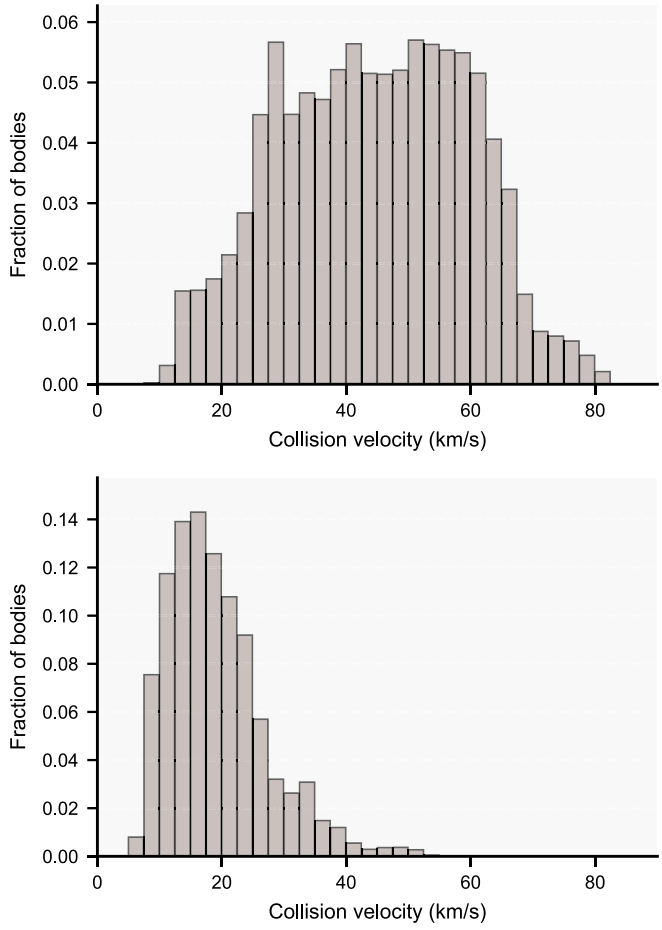

Fig. 1. Distribution of collision velocities between comets and Mars in J24 (top) and R25 (bottom). Collision velocities between each pair of bodies are weighted by the collision probability per unit of time at each possible collision orientation. The dynamical instability is more violent in J24, which leads to higher collision velocities.

rial *efficiently* accreted during the bombardment episode. This estimate is derived through a multi-step modeling framework that integrates: (1) the velocity distribution and impact probabilities of comets during the cometary bombardment phase; (2) the retention efficiency of cometary material depending on impactor sizes and velocities; (3) the size-frequency distribution and total mass of comets in the primordial trans-Neptunian disk; and (4) a correction for comet disruption effects. The total cometary mass efficiently accreted on Mars is given by:

$$m_{\text{comet}} = \sum_i M_{\text{tot}}(D \leq 100\ \text{km})\, p_{\text{coll}}\, f(D_i)\, \frac{\chi_i(D_i)}{\alpha\, \beta_i} \tag{1}$$

where each of these factors, including the total mass of comets smaller than 100 km in the primordial disk $M_{\text{tot}}(D \leq 100\ \text{km})$, the collision probability p_{coll}, size distribution (fraction of the total mass in each comet size-bin $f(D_i)$), retention efficiency $\chi_i(D_i)$, obliquity correction (α), and disruption factor (β_i) is introduced and detailed in the subsequent subsections. The last subsection presents an estimate of the minimal mass of Mars' primordial (solar-derived) atmosphere necessary to dilute cometary xenon signatures.

2.1. Velocity distribution and collision probability during the cometary bombardment

We first determined the velocity distribution $f(v_j)$ (Fig. 1) and average collision probability p_{coll} of comets impacting Mars during the cometary bombardment. This was achieved by combining N-body simulations of the early evolution of the solar system with an Öpik/Wetherill approach (Wetherill, 1967; Farinella and Davis, 1992; Bottke et al., 1994) - a semi-analytical method for computing collision probabilities and velocities between two bodies, based on their orbital elements and assuming random encounter geometries. Although the existence of a phase of dynamical instability of the giant planets, destabilizing the trans-Neptunian cometary disk, is well accepted, the dynamical character of the instability is not uniquely determined. Thus, to assess the sensitivity of our results to its dynamical properties, we used simulation outputs from two independent studies: Joiret et al. (2024), featuring a violent instability, and Ribeiro et al. (2025), featuring a milder instability, hereafter J24 and R25 respectively.

All simulations started at the time of gas disk dispersal (t_0) and spanned 100 Myr. In J24, simulations were performed using GENGA (Grimm and Stadel, 2014). Large bodies, including planetary embryos and planets, were treated with full gravity, while smaller bodies such trans-Neptunian objects were only influenced by massive objects. The primordial reservoir of trans-Neptunian objects was distributed between 21 and 30 AU, with a total mass of 25 $M_\oplus$. This configuration follows predictions from models of the early solar system's dynamical evolution (Nesvorný, 2018), which account for collisional losses within the primordial disk (Bottke et al., 2023). The outer disk was represented by 10^4 comets. To account for the effects of an *Early Instability* scenario (Clement et al., 2018), giant planets were forced into a dynamical instability ~ 2 Myr after gas disk dispersal. This was achieved using simulation outputs of giant planets evolution from Clement et al. (2021b).

In R25, simulations were performed using REBOUND (Rein and Liu, 2012). The reservoir of trans-Neptunian objects initially extended from about 22 to 30 AU, and comprised 10^6 massless, test particles. For computational efficiency, in the present study, we limited our analysis to 88,000 particles, corresponding to one in ten simulations from the original R25 dataset. Jupiter and Saturn were initially placed in their current orbits, while Uranus and Neptune were initially placed inside their current orbits and then forced to migrate outward (Nesvorný et al., 2017). The initial orbits of Uranus and Neptune were $a_U = 16$ AU, $e_U = 0$, $i_U = 0$, and $a_N = 24$ AU, $e_N = 0$, $i_N = 0$, respectively. The timing of the instability occurs at 10 Myr after gas disk dispersal.

It should be noted that the instability itself — that is, the evolution of the giant planets due to interactions with the massive outer disk — was modeled in earlier studies (e.g. Nesvorný and Morbidelli (2012) or Clement et al. (2021b). In J24 and R25, this interaction is not simulated directly; the resulting dynamical pathways are instead adopted from those prior models and applied to massless particles in order to study their dynamics and resulting bombardment (i.e. collision probability and velocity). Our results are not sensitive to the total mass of the primordial outer disk, but rather (as detailed below) to the size frequency distribution of comets. This is because massive objects that are not numerous enough to hit Mars with any significant probability (e.g. Pluto-size bodies) don't matter in our study, even if they can carry most of the mass of the disk.

We considered numerical outputs from both J24 and R25 to estimate the collision rate between comets and a Mars-like planet. The algorithm used for these collision rate calculations is described in detail in Joiret et al. (2024).

The average collision probability p_{coll} of comets impacting Mars during the cometary bombardment per comet initially in the trans-Neptunian disk is $\sim 10^{-6}$ in J24, and $\sim 3.1 \times 10^{-7}$ in R25. The latter is very close to the value of 3.3×10^{-7} found by Nesvorný et al. (2023). The more intense cometary bombardment in J24 is related to higher collision velocities, related to a more violent giant planet instability (in a medium with a given particle density, the collision probability is proportional to the relative velocity). However, these two factors —higher impact probabilities and reduced retention efficiencies due to faster impacts- are expected to roughly compensate with each other when considering the net mass of cometary material retained by Mars. This compensatory effect implies that our estimates are not highly sensitive to the specific dynamical scenario adopted, as shown below. Despite different dynami-

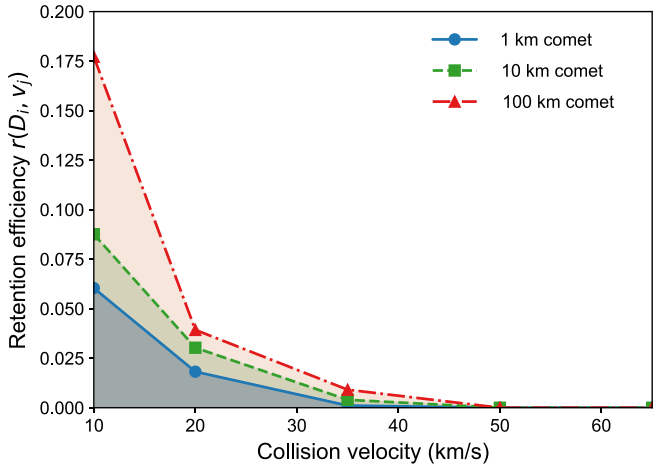

Fig. 2. Retention efficiency of cometary material on Mars across different impact velocities and comet sizes, obtained from iSALE2D simulations.

cal histories, both datasets yield comparable mass estimates of cometary material retained on Mars.

2.2. Retention efficiencies

We used hydrodynamic impact simulations to calculate the retention efficiency of cometary material on Mars (i.e. the mass of the cometary impactor that stays on the planet divided by the total mass of the impactor), $r(D_i, v_j)$, across a range of impactor sizes ($D_i = [1,\ 10,\ 100]$ km) and velocities ($v_j = [10,\ 20,\ 35,\ 50,\ 65]$ km/s). Fig. 2 summarizes the computed retention efficiencies for different impact conditions.

Impact simulations were performed using the iSALE2D shock physics code. The simulation domain was a two-dimensional box with cylindrical symmetry, featuring free-slip boundary conditions on the left and right, no-slip at the bottom, and an outflow condition at the top. The target was a basaltic Martian surface, modeled by the ANEOS using the default parameters in iSALE2D. Comets were assumed to be made of pure water ice, modeled by Tillotson equations of state (also using the default parameters in iSALE2D). Martian surface gravity was set at 3.72 m/s^2.

In our 2D simulations, all impacts are vertical. However, the most probable impact angle is 45° (Pierazzo and Melosh, 2000); and both laboratory experiments and 3D numerical simulations show that projectile retention decreases as the impact angle (measured from the horizontal) decreases (Pierazzo and Chyba, 2003; Daly and Schultz, 2016). To account for this discrepancy, we introduce a correction factor α, equal to 1.32, derived from comparative studies of cometary impacts on Mars performed both in 2D simulations and at oblique angles, including 45° in 3D simulations (Pierazzo and Chyba, 2003, 2006). The final estimate of the cometary mass efficiently retained on Mars should be divided by this correction factor. Although studies from (Pierazzo and Chyba, 2003, 2006) focus on relatively low-velocity impacts, the correction factor α offers a reasonable first-order estimate for angle-averaged retention efficiency. As illustrated in Fig. 2, retention of cometary material on Mars is largely dominated by low-velocity impacts. Most importantly, our aim is not to precisely model angle dependence, but to provide a broad estimate of the retained cometary mass. Applying this correction does not change our results at the order-of-magnitude level, and is chosen to ensure a conservative estimate.

Each simulation employed a resolution of 50 cells per projectile radius, corresponding to a grid spacing of 10 m, 100 m, and 1 km for 1-km, 10-km, and 100-km impactors, respectively. 50 CPPR is a good compromise between accuracy and computational cost. Also, this is consistent with prior studies that show convergence of global metrics for resolutions of 20 CPPR or higher (Pierazzo et al., 2008). All simulations began with the first contact between the projectile and the target and stopped after the collapse of the transient crater. We ensured that all simulations were run until the time evolution of ejected material asymptotically leveled off, indicating convergence. This plateau behavior confirms that the bulk of the impact processes had concluded and that the calculated retention efficiencies were not sensitive to longer run times. Figures that illustrate these asymptotic trends can be found in Supplementary Materials. Our initial approach was to estimate Xe loss by applying the Maxwell–Boltzmann distribution to the post-impact temperature distribution. However, peak temperatures never reached values high enough to accelerate Xe atoms beyond Mars' escape velocity, due to the high atomic mass of Xe. So instead, retention efficiency was computed by tracking the post-impact material distribution at each timestep and measuring the fraction of cometary mass that did not reach Mars' escape velocity.

Table 1
Fraction $\chi_i(D_i)$ of cometary material efficiently accreted on Mars for each diameter D_i of comets, shown for cases J24 and R25. Case R25 demonstrates a higher retention of cometary material, due to lower collision velocities.

	1 km	10 km	100 km
J24	0.31%	0.58%	0.89%
R25	2.41%	3.79%	6.20%

We note that our retention efficiencies for small impactors (e.g., 1 km at 20 km/s, see Fig. 2) are significantly lower than those reported in previous studies such as Svetsov (2007), who found that ∼ 90% of the impactor mass may be retained under similar impact conditions. This discrepancy is primarily due to the fact that such studies include the presence of a dense atmosphere using the SOVA code - which offers a better treatment of ablation than iSALE. Atmospheric drag and ablation significantly enhance retention for kilometer-size impactors. In our simulations, we neglected the presence of an atmosphere, which leads to an overestimation of cometary impact velocities and underestimation of the retention efficiencies (mainly in the case of smaller impactors). This is intentional: our objective is to determine a strict lower bound on the retained mass and on the Martian primordial atmosphere. Moreover, as we show in Section 2.3, the cometary bombardment was dominated in mass by impactors larger than ∼ 10 km, for which atmospheric effects are minimal.

Then, we studied the cumulative retention of all accreted cometary material by calculating the fraction $\chi_i(D_i)$ of cometary material efficiently accreted on Mars for each diameter D_i of comets, given a normalized velocity distribution $f(v_j)$ (Table 1):

$$\chi_i(D_i) = \sum_j r(D_i, v_j) f(v_j) \tag{2}$$

2.3. Mass of the continuous cometary bombardment

We derived the total mass of cometary material accreted on Mars from the *continuous* component of the bombardment — that is, the bombardment carried by objects that are numerous enough that their collision with Mars is certain (i.e. their number times their collision probability is significantly larger than 1). It turns out that the continuous component is carried by comets smaller than 100 km in diameter. The cumulative mass they carry to Mars is expressed as $M_{\rm tot}(D \leq 100\ {\rm km})\, p_{\rm coll}$, where $M_{\rm tot}(D \leq 100$ km) is the total mass of comets smaller than 100 km in the primordial trans-Neptunian disk and $p_{\rm coll}$ is the average collision probability of comets impacting Mars following the dynamical instability. The continuous component is complemented by the stochastic component, carried by large comets (those >100 km in diameter). The latter population was too rare (∼ 10^7 in the primordial trans-Neptunian

Table 2
Total mass $M_{\rm tot}(D \leq 100$ km) of comets smaller than 100 km and mass fraction $f(D_i)$ of comets of diameter D_i in the primordial trans-Neptunian disk (considering objects smaller than 100 km only), as calculated from the cumulative size distribution of primordial trans-Neptunian objects in Nesvorný et al. (2017).

$M_{tot}(D \leq 100$ km)	$f(D_i \sim 1$ km) $= \frac{M_{\rm tot}(D \leq 5\ {\rm km})}{M_{\rm tot}(D \leq 100\ {\rm km})}$	$f(D_i \sim 10$ km) $= \frac{M_{\rm tot}(5 < D \leq 50\ {\rm km})}{M_{\rm tot}(D \leq 100\ {\rm km})}$	$f(D_i \sim 100$ km) $= \frac{M_{\rm tot}(50 < D \leq 100\ {\rm km})}{M_{\rm tot}(D \leq 100\ {\rm km})}$
$\sim 5 \times 10^{28}$ g	6.6%	46.7%	46.7%

disk, Nesvorný et al. (2017)) for their impacts to be treated as a smooth flux, given the very low collision probabilities $p_{\rm coll} \sim 10^{-7}$-$10^{-6}$. Instead, such impacts would have occurred as isolated events rather than as a continuous process. Since our objective is to estimate a conservative lower bound on the mass contribution of the cometary bombardment to Mars' primordial atmosphere, we excluded this stochastic component from our calculations.

The total mass of comets smaller than 100 km in the primordial trans-Neptunian disk was determined using the cumulative size distribution $N(>D) \sim 10^{12}(\frac{D}{1\ {\rm km}})^{-2.1}$ from Nesvorný et al. (2017), which was inferred from present-day populations of Jupiter Trojans (D> 10 km) and Kuiper Belt Objects (D> 50 km), flux of Jupiter-family comets (D> 1 km) and based on the mass of the original disk needed to generate the plausible dynamical evolution of the solar system (Nesvorný and Morbidelli, 2012; Nesvorný and Vokrouhlický, 2016; Deienno et al., 2017). The corresponding differential size distribution is expressed as:

$$n(D)dD \sim C \times (\frac{D}{1\ {\rm km}})^{-3.1} dD \tag{3}$$

with C calculated as 2.1×10^{12}. The total mass of comets with diameters below 100 km, $M_{tot}(D \leq 100$ km), is obtained by integrating over the size distribution:

$$M_{tot}(D \leq 100\ {\rm km}) = \rho \int_0^{100} \frac{4}{3}\pi \left(\frac{D}{2}\right)^3 n(D)dD \simeq 5 \times 10^{28}\ {\rm g} \tag{4}$$

assuming a cometary bulk density ρ of 500 kg/m^3 (Richardson et al., 2007; Brown, 2013; Groussin et al., 2019), expressed in kg/km^3 in the calculations.

The mass fraction of comets within this size range in the primordial disk is then evaluated for three representative diameters (D_i = [1, 10, 100] km), as follows:

$$f(D_i \sim 1\ {\rm km}) = \frac{M_{\rm tot}(D \leq 5\ {\rm km})}{M_{\rm tot}(D \leq 100\ {\rm km})} \tag{5}$$

$$f(D_i \sim 10\ {\rm km}) = \frac{M_{\rm tot}(5 < D \leq 50\ {\rm km})}{M_{\rm tot}(D \leq 100\ {\rm km})} \tag{6}$$

$$f(D_i \sim 100\ {\rm km}) = \frac{M_{\rm tot}(50 < D \leq 100\ {\rm km})}{M_{\rm tot}(D \leq 100\ {\rm km})} \tag{7}$$

Results are summarized in Table 2.

2.4. Comet disruption

Comets tend to lose mass due to long-lasting activity and spontaneous disruption (Chen and Jewitt, 1994; Levison et al., 2002). Alternatively, they can become dormant due to the formation of a refractory crust that inhibits dust and volatile emissions (Coradini et al., 1997; Ye et al., 2016). If spontaneous comet disruption is taken into account, Nesvorný et al. (2023) showed that the impact flux of comets on Mars is reduced by a factor $\beta_{\rm i}$ = 36, 4.9 and 1.7 for comets of 1, 10 and 100 km in diameters, respectively.

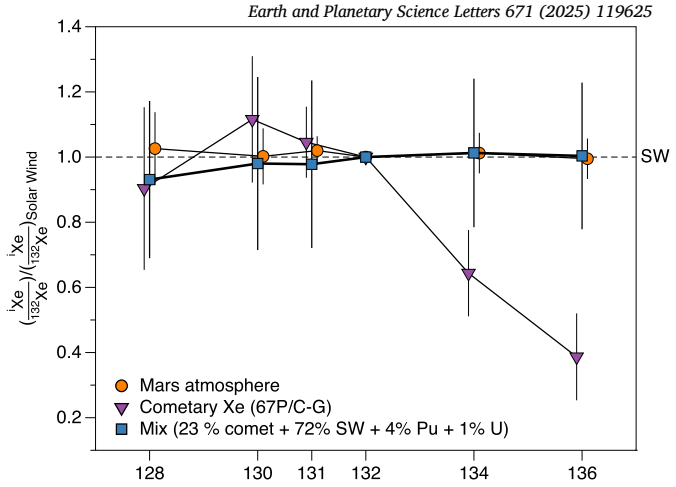

Fig. 3. A mixture of solar and cometary Xe as the origin of the primordial atmospheric Xe on Mars. The Xe isotopes are normalized to ^{132}Xe and the solar wind composition SW-Xe (the horizontal dashed line). SW-Xe data are from Meshik et al. (2020), Cometary (67P/Churyumov-Gerasimenko) data are from Marty et al. (2017) and Martian atmosphere data are from Conrad et al. (2016), corrected for mass-dependent fractionation. Xe production due to Pu-fission and U-fission is taken into account. Error bars are 1σ.

2.5. Minimal mass of the primordial atmosphere on Mars

Finally, by combining all the components described above, we obtain the expression for the total cometary mass efficiently accreted on Mars (Equation (1)):

$$m_{\rm comet} = \sum_i M_{\rm tot}(D \leq 100\ {\rm km})\, p_{\rm coll}\, f(D_i)\, \frac{\chi_i(D_i)}{\alpha\, \beta_i}$$

Taking into account comet disruption, we found $m_{\rm comet} = 1.1 \times 10^{20}$ g in the J24 case, and $m_{\rm comet} = 2.7 \times 10^{20}$ g in the R25 case. Neglecting it (i.e. setting $\beta_i = 1$), we found $m_{\rm comet} = 2.6 \times 10^{20}$ g in the J24 case, and $m_{\rm comet} = 5.4 \times 10^{20}$ g in the R25 case.

It remains possible that the Xe isotopic signature of the Martian atmosphere comprises a minor cometary contribution (Swindle and Jones, 1997; Marty et al., 2016). Using a Linear Least Squares fit combined with Monte Carlo error propagation (10^6 random iterations), we calculated that the Martian atmospheric xenon signature may comprise up to 16% cometary Xe for 82% solar Xe, accounting for the substantial measurement uncertainties in 67P/Churyumov-Gerasimenko. Forcing elevated rates of Xe production due to Pu-fission (e.g., $\sim$ 4%) increases the inferred cometary contribution (23% cometary Xe for 72% solar Xe, Fig. 3). Although there is no apparent evidence for Xe production due to Pu-fission (Conrad et al., 2016; Avice et al., 2018), this endmember scenario serves as an absolute lower bound on the solar-derived atmospheric component necessary to erase a cometary signature. Under this constraint, the solar-to-cometary Xe ratio is $\frac{72}{23} \simeq 3.1$.

The minimum mass of Mars' primordial atmosphere is thus the amount of solar nebular gas required to get at least 3.1× more solar Xe than cometary Xe. Given the fact that there is $\sim$ 100× more mass in the gaseous component of the solar nebula (mainly hydrogen and helium) than in its condensable (or dust) component (Pascucci and Tachibana, 2010), and that the Xe to condensable species ratio is 3× lower in comets than in the solar nebula (Marschall et al., 2025), we have:

$$m_{\rm atm,\ min} = m_{\rm gas,\ solar} = 100 \times m_{\rm cond,\ solar} = 100 \times m_{\rm Xe,\ solar} \times \left(\frac{m_{\rm cond}}{m_{\rm Xe}}\right)_{\rm solar}$$
$$\geq 100 \times 3.1 \times m_{\rm Xe,\ comet} \times \frac{1}{3} \times \left(\frac{m_{\rm cond}}{m_{\rm Xe}}\right)_{\rm comet} = 103.3\ m_{\rm cond,\ comet} \tag{8}$$

where $m_{\rm atm,\ min}$ is the minimum mass of the primordial Martian atmosphere, $m_{\rm gas,\ solar}$ is the mass of solar nebula gas that was accreted on

Mars and $m_{\text{cond, solar}}$ is the corresponding mass of condensable species in the solar nebula (that is, all species other than hydrogen and helium), $m_{\text{cond, comet}} \sim m_{\text{comet}}$ denotes the cometary mass, and $m_{\text{Xe, solar}}$ and $m_{\text{Xe, comet}}$ are the masses of Xe in the solar nebula and in comets, respectively.

Using the derived values, and taking into account comet disruption, the minimum mass of the primordial Martian atmosphere is estimated to be between approximately 1.1×10^{22} g and 2.8×10^{22} g, in the J24 and R25 cases, respectively, corresponding to surface pressures of 2.9 bar and 7.3 bar on Mars. Neglecting comet disruption, the minimal mass is estimated to be between approximately 2.7×10^{22} g and 5.6×10^{22} g, in the J24 and R25 cases, respectively, corresponding to surface pressures of 6.9 bar and 14.5 bar.

3. Discussion

To reconcile the estimated Ne abundances in the Martian mantle, Kurokawa et al. (2021) determined that the early Martian atmosphere would have required a Ne partial pressure of ~ 10 Pa. Assuming a ^{20}Ne molar fraction of 1.8×10^{-4} in the solar nebula, this corresponds to a total atmospheric pressure of ~ 0.5 bar (5×10^4 Pa) and an atmospheric mass of 2×10^{21} g. This estimate aligns with hydrodynamic simulations of solar nebula capture, which predict a primordial Martian atmosphere of at most 1 bar (Stökl et al., 2015). Our lower bound extends beyond this upper limit. Recent work showed that mixing an outgassed component (e.g., CO_2-rich) to the primordial H_2-rich atmosphere enhances the nebular captured gas inventory by $\sim$ 1–3 orders of magnitude (Pahlevan et al., 2025). In particular, for planetesimal accretion rates of 0.01–1 Mars masses/Myr (corresponding to different planetary luminosities) and heavy gas inventories equivalent to 10–1000 bars of CO_2 at the planetary surface (Elkins-Tanton, 2008), the captured nebula inventory is equivalent to $\sim$ 3–300 bars of H_2 at the surface. Such a hybrid primordial atmosphere is emerging as a compelling scenario, as it reproduces the noble gas isotopic composition observed in the Martian atmosphere (Pahlevan et al., 2025), including that of xenon.

An alternative, and arguably more natural, mechanism for increasing nebular gas retention involves H_2O vapor in equilibrium with a magma ocean. At the oxygen fugacity of the Martian mantle (IW $= 0 \pm 1$, Wadhwa (2008)), redox buffering between the atmosphere and interior imposes a $\log\left(f_{H_2O}/f_{H_2}\right)$ ratio of 0 ± 0.5 at 2000 K, raising the mean molecular weight from 2 to 10 ± 4 g/mol. This increase alone enhances the captured mass of nebular gas by up to an order of magnitude—potentially yielding 10–20 bars of H_2 at the surface. These values are in excellent agreement with those inferred from our method. This scenario invokes a (partial) magma ocean, which implies some exchange between the Martian atmosphere and interior. To preserve a chondritic Kr and Xe signature in the mantle, the amount of these gases dissolved during exchange must have been small - likely due to their low solubility relative to lighter noble gases (Carroll and Draper, 1994). In contrast, the higher solubility of He and Ne (despite their lower polarizabilities) makes their partial equilibration with the atmosphere more plausible (Kurokawa et al., 2021).

If the entire primordial atmosphere was lost through hydrodynamic escape within a few millions years (Erkaev et al., 2014), this would impose stringent constraints on the timing of cometary bombardment, as the isotopic signatures delivered by comets could no longer be diluted once the solar primordial atmosphere is gone. However, because atmospheric escape preferentially removes light species such as hydrogen and helium, heavier noble gases like xenon may persist longer. In this case, a residual solar Xe component could still buffer the isotopic signature of cometary Xe delivered after most of the atmosphere had been lost.

Alternatively, if the primordial atmosphere partially persisted over prolonged timescales, our results carry important implications for early Martian climate. The persistence of H_2-rich gases would represent a potent greenhouse contribution, potentially sustaining warmer surface conditions during the pre-Noachian era (Ramirez et al., 2014; Wordsworth et al., 2017; Hayworth et al., 2020; Turbet and Forget, 2021).

It should be noted that comets have much higher noble gas–to–H_2O, –C, and –N ratios than asteroids (Balsiger et al., 2015; Bekaert et al., 2020), allowing them to deliver substantial noble gases while contributing little H, C, or N compared to asteroids. This pattern is also seen on Earth, where the cometary contribution is negligible for water but significant for Ar, Kr, and Xe (Marty et al., 2016). While isotopic signatures of He, Ne, Ar, and Kr are less diagnostic than xenon, existing data suggest a cometary contribution to Mars's atmosphere remains plausible also for these elements. (Owen and Bar-Nun, 1995; Marty et al., 2016).

4. Conclusions

By combining noble gas data with N-body hydrodynamic impact simulations, we have quantified the minimal mass of Mars' primordial atmosphere necessary to retain a predominantly solar noble gas signature despite subsequent cometary impacts. Our findings imply that Mars accreted a substantial gaseous envelope from the solar nebula, with minimum surface pressures ranging from 2.9 to 14.5 bar — depending on the intensity of cometary bombardment and whether comet disruption is accounted for. These estimates are consistent with previous studies showing that the presence of heavier molecular species can significantly enhance nebular gas retention by increasing the mean molecular weight of the atmosphere (Kurokawa et al., 2021; Pahlevan et al., 2025). Whether Mars partially retained or rapidly lost its primordial atmosphere yields distinct interpretations. A rapid loss would limit the dilution from late-arriving comets, though a residual solar Xe component -less affected by atmospheric loss than hydrogen- may have persisted. In contrast, sustained retention of H_2-rich gases would have provided a substantial greenhouse warming, with profound implications for the pre-Noachian climate.

CRediT authorship contribution statement

Sarah Joiret: Writing – review & editing, Writing – original draft, Visualization, Investigation, Formal analysis, Data curation. **Alessandro Morbidelli:** Supervision, Methodology, Formal analysis, Writing – review & editing. **Rafael de Sousa Ribeiro:** Resources, Writing – review & editing. **Guillaume Avice:** Methodology, Visualization, Writing – review & editing. **Paolo Sossi:** Investigation, Writing – review & editing.

Declaration of competing interest

The authors declare that they have no known competing financial interests or personal relationships that could have appeared to influence the work reported in this paper.

Acknowledgements

We gratefully acknowledge David Nesvorný and Martin Turbet for their valuable insights, which greatly contributed to the advancement of this work. Computer time for this study was partly provided by the computing facilities MCIA (Mésocentre de Calcul Intensif Aquitain) of the Université de Bordeaux and of the Université de Pau et des Pays de l'Adour, France. Numerical computations were also partly performed on the S-CAPAD/DANTE platform, IPGP, France. This project has received funding from the European Research Council (ERC) under the European Union's Horizon Europe research and innovation program (grant agreement no. 101041122 to G.A.). RR thanks the scholarship granted from the Brazilian Federal Agency for Support and Evaluation of Graduate Education (CAPES), in the scope of the Program CAPES-PrInt (Proc 88887.310463/2018-00, Mobility number 88887.572647/2020-00, 88887.468205/2019-00). This research was supported in part by

the São Paulo Research Foundation (FAPESP) through the computational resources provided by the Center for Scientific Computing (NCC/GridUNESP) of the São Paulo State University (UNESP). RR also acknowledges support provided by grants FAPESP (Proc 2016/24561-0) and by São Paulo State University (PROPe 13/2022).

Appendix A. Supplementary material

Supplementary material related to this article can be found online at https://doi.org/10.1016/j.epsl.2025.119625.

Data availability

Data will be made available on request.

References

Avice, G., Bekaert, D.V., Aoudjehane, H.C., Marty, B., 2018. Geochem. Perspect. Lett.
Balsiger, H., Altwegg, K., Bar-Nun, A., et al., 2015. Sci. Adv. 1, e1500377.
Bekaert, D.V., Broadley, M.W., Marty, B., 2020. Sci. Rep. 10, 5796.
Bottke, W.F., Nolan, M.C., Greenberg, R., Kolvoord, R.A., 1994. Icarus 107, 255.
Bottke, W.F., Vokrouhlický, D., Marshall, R., et al., 2023. Planet. Sci. J. 4, 168.
Brown, M.E., 2013. Astrophys. J. Lett. 778, L34.
Carroll, M.R., Draper, D.S., 1994. Chem. Geol. 117, 37.
Chen, J., Jewitt, D., 1994. Icarus 108, 265.
Clement, M., Kaib, N.A., Raymond, S.N., Walsh, K.J., 2018. Icarus 311, 340.
Clement, M.S., Deienno, R., Kaib, N.A., et al., 2021b. Icarus 367.
Conrad, P.G., Malespin, C.A., Franz, H.B., et al., 2016. Earth Planet. Sci. Lett. 454, 1.
Coradini, A., Capaccioni, F., Capria, M.T., et al., 1997. Icarus 129, 337.
Daly, R.T., Schultz, P.H., 2016. Icarus 264, 9.
Dauphas, N., Pourmand, A., 2011. Nature 473, 489.
Deienno, R., Morbidelli, A., Gomes, R.S., Nesvorný, D., 2017. Astron. J. 153, 153.
Elkins-Tanton, L., 2008. Earth Planet. Sci. Lett. 271, 181.
Erkaev, N.V., Lammer, H., Elkins-Tanton, L.T., et al., 2014. Planet. Space Sci. 98, 106.
Farinella, P., Davis, D.R., 1992. Icarus 97, 111.
Gomes, R., Levison, H.F., Tsiganis, K., Morbidelli, A., 2005. Nature 435, 466.
Grimm, S.L., Stadel, J.G., 2014. Astrophys. J. 796, 23.
Groussin, O., Attree, N., Brouet, Y., et al., 2019. Space Sci. Rev. 215, 29.
Haisch Jr., K.E., Lada, E.A., Lada, C.J., 2001. Astrophys. J. Lett. 553, L153.
Hayworth, B.P.C., Kopparapu, R.K., Haqq-Misra, J., et al., 2020. Icarus 345, 113770.
Joiret, S., Raymond, S.N., Avice, G., Clement, M.S., 2024. Icarus 414, 116032.
Joiret, S., Raymond, S.N., Avice, G., et al., 2023. Icarus 406, 115754.
Kurokawa, H., Miura, Y.N., Sugita, S., et al., 2021. Icarus 370, 114685.
Levison, H.F., Morbidelli, A., Dones, L., et al., 2002. Science 296, 2212.
Marschall, R., Morbidelli, A., Marrocchi, Y., 2025. arXiv:2501.17864.
Marty, B., Altwegg, K., Balsiger, H., et al., 2017. Science 356, 1069.
Marty, B., Avice, G., Sano, Y., et al., 2016. Earth Planet. Sci. Lett. 441, 91.
Mathew, K.J., Kim, J.S., Marti, K., 1998. M&PS 33, 655.
Meshik, A., Pravdivtseva, O., Burnett, D., 2020. GeoCoA 276, 289.
Nesvorný, D., 2018. Annu. Rev. Astron. Astrophys. 56, 137.
Nesvorný, D., Morbidelli, A., 2012. Astron. J. 144, 117.
Nesvorný, D., Roig, F.V., Vokrouhlický, D., et al., 2023. Icarus 399, 115545.
Nesvorný, D., Vokrouhlický, D., 2016. Astrophys. J. 825, 94.
Nesvorný, D., Vokrouhlický, D., Dones, L., et al., 2017. Astrophys. J. 845, 27.
Ott, U., 1988. GeoCoA 52, 1937.
Owen, T., Bar-Nun, A., 1995. Icarus 116, 215.
Pahlevan, K., Schaefer, L., Porcelli, D., 2025. Geochemical perspectives letters. arXiv:2410.15508.
Pascucci, I., Tachibana, S., 2010. In: Apai, D.A., Lauretta, D.S. (Eds.), Protoplanetary Dust: Astrophysical and Cosmochemical Perspectives, pp. 263–298.
Pepin, R.O., 1992. Annu. Rev. Earth Planet. Sci. 20, 389.
Péron, S., Mukhopadhyay, S., 2022. Science 377, 320.
Pierazzo, E., Artemieva, N., Asphaug, E., et al., 2008. Meteorit. Planet. Sci. 43, 1917.
Pierazzo, E., Chyba, C., 2003. In: Lunar and Planetary Science XXXIV.
Pierazzo, E., Chyba, C.F., 2006. In: Comets and the Origin and Evolution of Life (Springer), pp. 137–168.
Pierazzo, E., Melosh, H.J., 2000. Annu. Rev. Earth Planet. Sci. 28, 141.
Ramirez, R.M., Kopparapu, R., Zugger, M.E., et al., 2014. Nat. Geosci. 7, 59.
Rein, H., Liu, S.F., 2012. Astron. Astrophys. 537, A128.
Ribeiro, R., Izidoro, A., Morbidelli, A., Nesvorny, D., Cabo Winter, O., 2025. arXiv:2501.17129.
Richardson, J.E., Melosh, H.J., Lisse, C.M., Carcich, B., 2007. Icarus 190, 357.
Stökl, A., Dorfi, E., Lammer, H., 2015. Astron. Astrophys. 576, A87.
Svetsov, V.V., 2007. Sol. Syst. Res. 41, 28.
Swindle, T.D., Jones, J.H., 1997. J. Geophys. Res. 102, 1671.
Tsiganis, K., Gomes, R., Morbidelli, A., Levison, H.F., 2005. Nature 435, 459.
Turbet, M., Forget, F., 2021. arXiv:2103.10301.
Wadhwa, M., 2008. Rev. Mineral. Geochem. 68, 493.
Wang, H., Weiss, B.P., Bai, X.-N., et al., 2017. Science 355, 623.
Weiss, B.P., Bai, X.-N., Fu, R.R., 2021. Sci. Adv. 7, eaba5967.
Wetherill, G.W., 1967. J. Geophys. Res. 72, 2429.
Wordsworth, R., Kalugina, Y., Lokshtanov, S., et al., 2017. Geophys. Res. Lett. 44, 665.
Ye, Q.-Z., Brown, P.G., Pokorný, P., 2016. Mon. Not. R. Astron. Soc. 462, 3511.